J Ther Eng, Vol. 12, No. 1, pp. 1−13, January, 2026

Journal of Thermal Engineering
Web page info: https://jten.yildiz.edu.tr
DOI: 10.14744/thermal.0001077

Journal of Thermal Engineering

Research Article

Thermo-diffusion effects on mhd casson blood flow in an inclined muti-stenosed artery

Harshad PATEL[1,*], Snehal PATEL[1], Nilesh PATEL[2]

[1]U V Patel College of Engineering, Ganpat University, Mehsana, Gujarat, 384012, India
[2]B. S. Patel Polytechnic, Ganpat University, Gujarat, 384012, India

ARTICLE INFO

Article history
Received: 13 May 2024
Revised: 26 July 2024
Accepted: 04 August 2024

Keywords:
Casson Fluid; Fractional Derivative; Magnetic Particles; MHD; Multi-Stenosed Artery; Thermal Radiation

ABSTRACT

The current study investigates the effects of thermos-diffusion on Casson blood flow in the presence of a magnetic field. We consider the flow in an inclined multi-stenosed artery with an oscillating pressure gradient. By using the similarity transformation, the governing equations are transformed into a dimensionless form. For more effective study of the fractional time derivative, the Caputo-Fabrizio time derivative is adopted. Using the tools provided by the Laplace transform and the finite Hankel transform, the analytical solution to the aforementioned problem is derived. We gather numerical findings and display them through graphs to help you better comprehend the effects of various physical parameters. Data visualization shows that the external magnet-controlled blood flow's turbulence. These results suggest that high magnetic field impacts are harmful to health. Additionally, it is observed that thermal radiation commonly enhances the heat distribution procedure.

Cite this article as: Patel H, Patel S, Patel N. Thermo-diffusion effects on mhd casson blood flow in an inclined muti-stenosed artery. J Ther Eng 2026;12(1):1−13.

INTRODUCTION

In contrast to the linear dependency shown by Newtonian fluids, the stress in non-Newtonian fluids can show a nonlinear rate of deformation. According to the literature, from the 1940s and 1950s, there has been an increase in interest in non-Newtonian fluids. Non-Newtonian fluids include things like paint, shampoo, soap slurries, tomato paste, greases, food sauces, chocolates, toothpaste, polymer solutions, custard, and blood. Non-Newtonian fluid models have been the subject of much study by numerous academics because of its applicability in numerous industries. Casson [1] developed the Casson fluid model in 1959 to determine how pigment oil suspensions would flow. Human red blood cells, human blood can also be considered as Casson fluid. Because blood is such a vital fluid, its viscosity and other characteristics can be used to detect a wide range of cardiovascular disorders. A great number of theoretical investigations [2-5] have been discussed blood flow circulation in the arteries. It is generally recognized that in sick conditions, an aberrant and unnatural growth arises in the lumen at numerous places throughout the circulatory system. Arteriosclerosis, often known as stenosis, is a common condition. Chaturani and

***Corresponding author.**
*E-mail address: harshadpatel2@gmail.com

This paper was recommended for publication in revised form by Editor-in-Chief Ahmet Selim Dalkilic

Ponnalagar Samy [6] have studied how blood moves via a stenosed artery. Many researchers [7-9] have investigated to impact of stenosis in the lumen of an artery. Casson's equation is obeyed by blood only for modest shear rate flows, according to Scott Blair et al. [10]. Shukla et al. [11] analysed the effects of stenosis on blood flow which is treated as a power-law and Casson's fluid.

Important applications of magnetic fields include the targeting of cancer drugs, the use of heat to kill tumors, magnetic resonance imaging (MRI), and magneto-therapy. In all these treatments effect of magnetic field plays crucial role. It is currently believed that magnetohydrodynamics (MHD) influences blood flows, or ionic flows, in a manner consistent with the bloodstream. In 1970, Hannes Alfvén [7] was awarded the Nobel Prize in physics for pioneering the field of MHD. The study of blood flow under the effect of magnetic field comes under the title Bio-magnetic fluid dynamics (BFD). Researchers [8-9] are curious about bio-magnetic fluid because Hyperthermia cell death, magnetic drugs targeting, magnetic endoscopy, magnetic devices for cell separation, therapy of cancer tumors, regulation of blood flow during surgery, and many more applications can be found in bioengineering. In the past few decades, the radiation therapy is used in human life where heat is transmitted below the skin's surface into the tissues and muscles [10-11]. Mekheiner and Kot [12] theoretically addressed the issue of blood flow through a catheterized artery under pathological conditions. To better understand the dynamics of blood flow via stenotic arteries, Majee and Shit [13] conducted a computer study of heat transfer in an unsteady blood flow. Both Rao and Vardynyan [14] demonstrated mathematically that blood can flow through an artery. Very few studies have looked at the effects of different parameter on blood flow and even fewer have taken into account fractional-order derivatives. However, the finite Hankel and Laplace transforms can be used to quickly find exact solutions to this type of problem. Caputo fractional derivatives and Hankel Transform methods are discussed to find the solution by researchers [15-17]. Due to its significance in physiopathology, problems with peristalsis (blood flow) have garnered a lot of attention. Mekheiner [18] determined that the pressure acts as an increasing function, but the behaviour of the pair stress fluid parameter appears to be the complete reverse. In his study, Akbar [19] examined the Prandtl fluid model in a tapering stenosed artery. The pumping features of peristaltic flow were discussed by Sreenadh et al. [20]. The slip effects for the flows investigated by Ramesh and Devakar [21], who then derived analytical solutions.

Nanofluid flow onto a stretched, curved surface was studied by Mehdi Mahboobtosi et al. [22] As a unique breakthrough, Moghimi et al. [23] analysed nanofluid flow in a channel and added magnetic field power to momentum and energy equations and evaluated free convection heat transmission. In a non-premixed configuration and in non-adiabatic conditions, Akbari et al. [24] conducted a theoretical analysis of a counter-flow combustion system that is powered by porous biomass particles. Using the response surface method, Navid et al. [25] optimized a wavy trapezoidal porous cavity that contained a mixture of hybrid nanofluids. Using computational methods, Zangooee et al. [26] examined the mixed nanofluid (NF) flow between two overlapping cylinders. Hosseinzadeh et al. [27] examined the thermal performance of a ferrofluid-wetted hybrid nanofluid with varying cross-sections in a moving porous fin subjected to a magnetic field. Hosseinzadeh et al. [28] studied the flow of a TiO2-ethylene glycol nanofluid across a porous stretched sheet under convective boundary conditions and the presence of heat that is not uniformly generated or absorbed. Muddasar Gulzar et al. [29] presented a nonlinear mathematical analysis of magneto-hyperbolic-tangent liquids that involve the three interrelated concepts of a magnetic field, a heat source, and thermal stratification. As a non-Newtonian fluid moving inside an axisymmetric tube subjected to non-uniform surface heat flux, Shahin Faghiri et al. [30] studied the Graetz-Nusselt problem for blood. Tashtoush et al. [31] presented a mathematical model of in-arterial multi-stenosis. The effects of a magnetic field on the heat and fluid flow properties of blood flowing through arteries with multiple stenosis are taken into account.

In light of what has been said previously, the objective of this investigation is to look into the impact that heat and mass transfer with thermal radiation and thermos-diffusion effects on blood flow in multi-stenosed artery. A thorough search of the relevant literature has witnessed the fact that the existing literature did not present the exact solution of MHD blood flow model in the context of Caputo Fabrizio fractional derivative for inclined multi-stenosed artery. The exact solutions are then calculated by means of significant transformations like Laplace and finite Hankel transforms. For numerical computations, we take the zeros of the Bessel functions to generate the graphical findings by using Matlab for different values of fractional parameters as well as some important physical parameters.

The present work furnishes a robust benchmark for magneto-hemodynamics, biomedical engineering, and physiology.

MATHEMATICAL FORMULATION

The focus of the recent research works is discussed on unsteady Casson blood flow, whose physical dimension are as shown in Figure 1. In Figure 1, z-axis consider as axial direction while r-axis indicates radial direction. Blood is treated as non-Newtonian Casson fluid flow with oscillating pressure gradient. The uniform external magnetic fields B_0 is applied which is shown in Figure 1. At $t = 0$, the velocity of blood and magnetic particle are treated as stationary. Blood flow is modelled using Navier-stokes equation. The effects of magnetic fields by Maxwell's relation whereas, magnetic particle velocity is governed using Newton's second law.

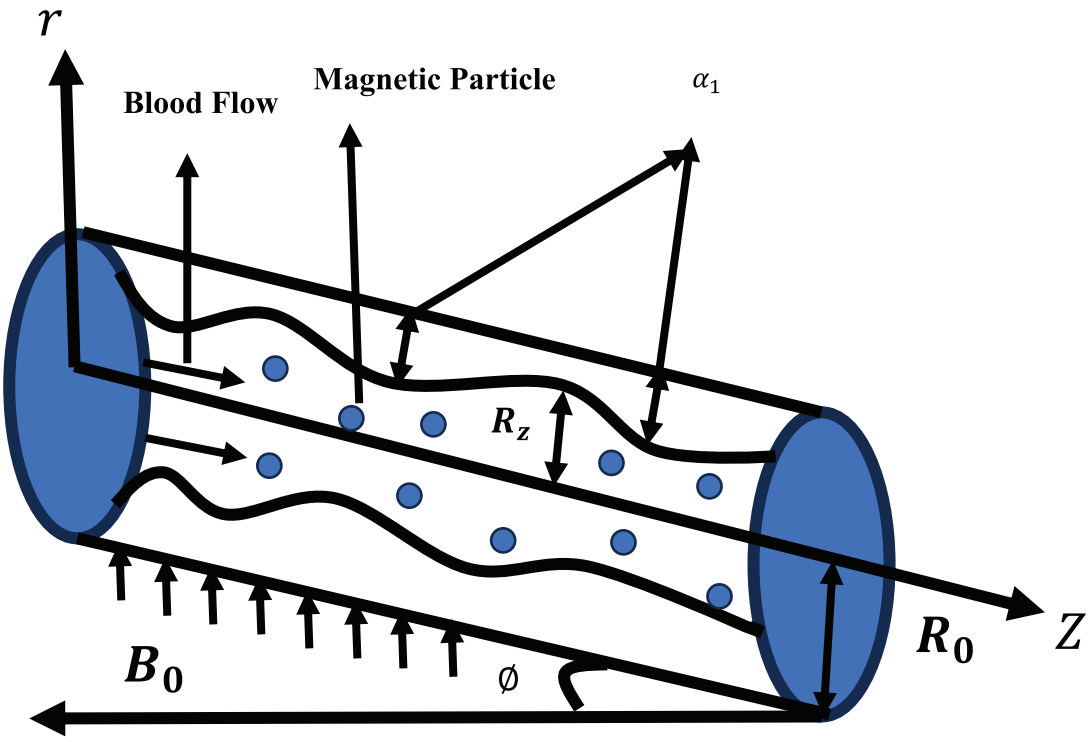

Figure 1. Geometry of the model

The unsteady blood flow in an axisymmetric cylindrical tube of radius R_0 under the influence of uniform transverse magnetic field and pressure gradient of the form [31].

$$-\frac{\partial P}{\partial z} = a_0 + a_1 Cos\,(\omega t), a_0 > 0 \tag{1}$$

Where, a_0- systolic pressure gradient, a_1-diastolic pressure gradient.

Geometrically, the expression of multi-stenosis in the artery can be written mathematically [32]

$$\begin{aligned} R_z = 1 - \alpha_1\,(&1.48x - 0.739x^2 + 0.148x^3 \\ &- 0.013955x^4 + 0.0006145x^5 \\ &- 0.000010243x^6) \end{aligned} \tag{2}$$

Where, R_z and R_0 represent the constricted region and normal artery radius. x is the stenosed length and α_1 stenosis degree.

The momentum equation for fluid flow in an inclined stenosed artery [15-33] can be written as

$$\begin{aligned} \frac{\partial u}{\partial t} = &-\frac{1}{\rho}\frac{\partial p}{\partial z} + \nu\left(1 + \frac{1}{\gamma}\right)\left(\frac{\partial^2 u}{\partial r^2} + \frac{1}{r}\frac{\partial u}{\partial r}\right) \\ &+ \frac{KN}{\rho}(v - u) - \frac{\sigma {B_0}^2 sin\theta_1}{\rho}u + gsin\emptyset \end{aligned} \tag{3}$$

The term $\frac{KN}{\rho}(v-u)$ is the force due to the relative motion between fluid and magnetic particles. It is assumed that the Reynolds number of the relative velocity is small. As such, the force between the magnetic particles and the blood is proportional to the relative velocity. Using Newton's second law governs the movement of magnetic particles:

$$m\frac{\partial v}{\partial t} = K\,(u - v) \tag{4}$$

where m is the average mass of the magnetic particles.

The governing energy equation in the cylindrical form as,

$$\frac{\partial T}{\partial t} = \frac{K_1}{\rho C_p}\left(\frac{\partial^2 T}{\partial r^2} + \frac{1}{r}\frac{\partial T}{\partial r}\right) + \frac{Q_m + \theta_m}{\rho C_p} \tag{5}$$

The concentration equation in the cylindrical form as,

$$\frac{\partial C}{\partial t} = D_m\left(\frac{\partial^2 C}{\partial r^2} + \frac{1}{r}\frac{\partial C}{\partial r}\right) + \frac{D_m K_T}{T_\infty}\left(\frac{\partial^2 T}{\partial r^2} + \frac{1}{r}\frac{\partial T}{\partial r}\right) \tag{6}$$

With initial and boundary conditions are as,

$$\begin{aligned} &u(r,0) = v(r,0) = T(r,0) = C(r,0) = 0 \;at\; r \in [0, R_z] \\ &u(r,t) = v(r,t) = T(r,t) = C(r,0) = 0 \;at\; r = R_z \end{aligned} \tag{7}$$

The dimensionless parameters can be express as,

$$r^* = \frac{r}{R_0},\; t^* = \frac{t}{\lambda},\; u^* = \frac{u}{u_0},\; {a_0}^* = \frac{\lambda a_0}{\rho u_0},$$

$${a_1}^* = \frac{\lambda a_1}{\rho u_0},\; \omega^* = \lambda\omega,\; g^* = \frac{g}{\frac{u_0^2}{R_0}}$$

The governing dimensionless form of governing equation subject to equations (7) after dropping* notation and

consider the time-fractional model of governing equations 3-6 can be written as,

$$D_t^{\alpha}u = a_0 + a_1\cos(\omega t) + \frac{1}{R_e}\left(1+\frac{1}{\gamma}\right)\left[\frac{\partial^2 u}{\partial r^2}+\frac{1}{r}\frac{\partial u}{\partial r}\right] + R(v-u) - Ha^2 u + \frac{\sin\emptyset}{F} \tag{8}$$

$$\mathrm{G}D_t^{\alpha}v = u - v \tag{9}$$

$$P_e D_t^{\alpha}\theta = \left(\frac{\partial^2\theta}{\partial r^2}+\frac{1}{r}\frac{\partial\theta}{\partial r}\right) + P_e(Q_m+\theta_m) \tag{10}$$

$$S_c\, R_e D_t^{\alpha}\, C = \left(\frac{\partial^2 C}{\partial r^2}+\frac{1}{r}\frac{\partial C}{\partial r}\right) + S_r\, S_c\left(\frac{\partial^2\theta}{\partial r^2}+\frac{1}{r}\frac{\partial\theta}{\partial r}\right) \tag{11}$$

With boundary conditions

$$\begin{aligned} &u\left(\frac{r}{R_z},0\right)=0\,,v\left(\frac{r}{R_z},0\right)=0\,,\theta\left(\frac{r}{R_z},0\right)=0\ \&\\ &C\left(\frac{r}{R_z},0\right)=0\ \ at\ \frac{r}{R_z}\in[\,0\,,1]\\ &u\left(\frac{r}{R_z},t\right)=0\,,v\left(\frac{r}{R_z},t\right)=0\,,\theta\left(\frac{r}{R_z},t\right)=0\ \&\\ &C\left(\frac{r}{R_z},t\right)=0\ at\ \frac{r}{R_z}=\ 1 \end{aligned} \tag{12}$$

Here, $\beta=\frac{1}{R_e}\left(1+\frac{1}{\gamma}\right), Ha=B_0\sqrt{\lambda}\sqrt{\frac{\sigma sin\theta_1}{\rho}}$,

$F=\frac{R_0}{\lambda u_0 g}\,,\theta=\frac{T-T_\omega}{T_\omega-T_\infty}\,,\ P_r=\frac{K\lambda}{\rho C_p},\ R_e=\frac{{R_z}^2}{\lambda v}\,,$

$P_e=R_e.P_r,\ S_c=\frac{v}{\lambda D_m}\,,C=\frac{C-C_\omega}{C_\omega-C_\infty}\ S_r=\frac{D_m K_T\,(T_\omega-T_\infty)}{\lambda v\, T_\infty\,(C_\omega-C_\infty)},$

$Q_m=\frac{R_0\overline{Q_m}}{\lambda\, u_0\rho c_p(T_\omega-T_\infty)}\,,\ \theta_m=\frac{R_0\overline{\theta_m}}{\lambda\, u_0\rho c_p(T_\omega-T_\infty)}$

Solution of the Problem

The Laplace transform technique is applied in equations (10), we obtain

$$P_e\frac{S\,\theta(r,s)}{S+\alpha(1-s)} = \left[\frac{\partial^2\theta(r,s)}{\partial r^2}+\frac{1}{r}\frac{\partial\theta(r,s)}{\partial r}\right] + P_e\frac{Q_m+\theta_m}{S} \tag{13}$$

The FHT (Finite Hankel transformation) is applied in equations (13) with B.C. (12),

$$P_e\frac{S\,\overline{\theta_H}(r_n,s)}{S+\alpha(1-s)} = -r_n\overline{\theta_H}(r_n,s) + P_e\frac{Q_m+\theta_m}{S}.\frac{J_1(r_n)}{r_n} \tag{14}$$

$$\overline{\theta_H}(r_n,s) = \frac{P_e\,(Q_m+\theta_m)}{S\left[r_n+P_e\frac{S}{S+\alpha(1-s)}\right]}.\frac{J_1(r_n)}{r_n} \tag{15}$$

Now, rearrange the equation (15)

$$\overline{\theta_H}(r_n,s) = \left[\frac{1}{S+B_{15}}B_{13}+\frac{1}{s\,(S+B_{15})}B_{14}\right]\frac{J_1(r_n)}{r_n} \tag{16}$$

Similarly, we process for Concentration equation (11), we get

$$R_e S_c\,\frac{S\,\bar{C}(r,s)}{S+\alpha(1-s)} = \left(\frac{\partial^2\bar{C}(r,s)}{\partial r^2}+\frac{1}{r}\frac{\partial\bar{C}(r,s)}{\partial r}\right) + S_r\,S_c\left(\frac{\partial^2\bar{\theta}(r,s)}{\partial r^2}+\frac{1}{r}\frac{\partial\bar{\theta}(r,s)}{\partial r}\right) \tag{17}$$

The FHT (Finite Hankel transformation) is applied in equations (17) with B.C. (12),

$$R_e S_c\,\frac{S\,C_H(r,s)}{S+\alpha(1-s)} = -r_n\overline{C_H}(r_n,s) + S_r\,S_c\,(-r_n)\overline{\theta_H}(r_n,s) \tag{18}$$

$$R_e S_c\,\frac{S\,C_H(r,s)}{S+\alpha(1-s)} = -r_n\overline{C_H}(r_n,s) + S_r\,S_c\,(-r_n)\frac{P_e\,(Q_m+\theta_m)}{S\left[r_n+P_e\frac{S}{S+\alpha(1-s)}\right]}.\frac{J_1(r_n)}{r_n} \tag{19}$$

$$\left[\frac{R_e S_c.S}{S+\alpha(1-s)}+r_n\right]\overline{C_H}(r,s) = -\,r_n S_r\,S_c\left[\frac{P_e\,(Q_m+\theta_m)}{S\left[r_n+P_e\frac{S}{S+\alpha(1-s)}\right]}\right].\frac{J_1(r_n)}{r_n} \tag{20}$$

$$\overline{C_H}(r,s) = -\frac{S_r\,S_c\,r_n P_e\,(Q_m+\theta_m)}{\left(S\left[r_n+P_e\frac{S}{S+\alpha(1-s)}\right]\right)\left[\frac{R_e S_c.S}{S+\alpha(1-s)}+r_n\right]}.\frac{J_1(r_n)}{r_n} \tag{21}$$

Now, rearrange the equation (21)

$$\overline{C_H}(r,s) = \frac{B_{16}}{\left(S\left[B_{17}+P_e\frac{S}{S+\alpha(1-s)}\right]\right)\left[\frac{B_{19}.S}{S+\alpha(1-s)}+B_{18}\right]}.\frac{J_1(r_n)}{r_n} \tag{22}$$

$$\overline{C_H}(r,s) = \frac{B_{16}\,(S+\alpha(1-S))^2}{S\,(B_{17}S+B_{17}\alpha-B_{17}\alpha S+P_e S)(B_{19}S+B_{18}\alpha+B_{18}S-B_{18}\alpha S)}.\frac{J_1(r_n)}{r_n} \tag{23}$$

$$\overline{C_H}(r,s) = \frac{B_{16}\,(S+\alpha(1-S))^2}{S\,((B_{17}-B_{17}\alpha+P_e)S+B_{17}\alpha)((B_{19}+B_{18}-B_{18}\alpha)S+B_{18}\alpha)}.\frac{J_1(r_n)}{r_n} \tag{24}$$

$$\overline{C_H}(r,s) = \frac{B_{16}\,(S+\alpha(1-S))^2}{S\,(B_{20}S+B_{22})(B_{21}S+B_{23})}.\frac{J_1(r_n)}{r_n} \tag{25}$$

$$\overline{C_H}(r,s) = \frac{B_{16}}{B_{20}.B_{21}}\frac{(\alpha^2+2\alpha(1-\alpha)S+(1-\alpha)^2S^2)}{S\left(S+\frac{B_{22}}{B_{20}}\right)\left(S+\frac{B_{23}}{B_{21}}\right)}.\frac{J_1(r_n)}{r_n} \tag{26}$$

$$\overline{C_H}(r,s) = \frac{B_{24}\,(\alpha^2+B_{25}S+B_{26}S^2)}{S\,(S+B_{27})\,(S+B_{28})}.\frac{J_1(r_n)}{r_n} \tag{27}$$

$$\overline{C_H}(r,s) = \left(\frac{B_{29}}{S}+\frac{B_{30}}{S+B_{27}}+\frac{B_{29}}{S+B_{28}}\right).\frac{J_1(r_n)}{r_n} \tag{28}$$

Now, the Laplace transform of equations (8) and (9) can be express as,

$$\frac{S\,\overline{u}(r,s)}{S+\alpha(1-s)} = \frac{a_0}{S}+\frac{a_1 S}{s^2+\omega^2}+\gamma\left(\frac{\partial^2\overline{u}(r,s)}{\partial r^2}+\frac{1}{r}\frac{\partial\overline{u}(r,s)}{\partial r}\right) + R\bar{v} - (R+Ha^2)\overline{u}(r,s) + \frac{\sin\emptyset}{SF} \tag{29}$$

$$G\frac{S\,\bar{v}(r,s)}{S+\alpha(1-s)} = \bar{u}(r,s) - \bar{v}(r,s) \tag{30}$$

$$\bar{v}(r,s) = \frac{S+\alpha(1-\alpha)}{GS+S+\alpha(1-s)}\,\bar{u}(r,s) \tag{31}$$

Input the equation (31) in (29), the following equation can be obtained,

$$\left[\frac{s}{S+\alpha(1-S)} - R\left(\frac{S+\alpha(1-\alpha)}{GS+S+\alpha(1-s)}\right) + R + Ha^2\right]\bar{u}(r,s) = \frac{a_0}{S} + \frac{a_1 S}{s^2+\omega^2} + \gamma\left(\frac{\partial^2\bar{u}}{\partial r^2} + \frac{1}{r}\frac{\partial\bar{u}}{\partial r}\right) + \frac{sin\phi}{SF} \tag{32}$$

The FHT (Finite Hankel transformation) is applied in equations (32) with B.C. (12),

$$\left[\frac{s}{S+\alpha(1-S)} - R\left(\frac{S+\alpha(1-\alpha)}{GS+S+\alpha(1-s)}\right) + R + Ha^2\right]\overline{u_H}(r_n,s) = \left[\frac{a_0}{S} + \frac{a_1 S}{s^2+\omega^2} + \frac{sin\phi}{SF}\right]\frac{J_1(r_n)}{r_n} - r_n\gamma\overline{u_H}(r_n,s) \tag{33}$$

$$\overline{u_H}(r_n,s) = \frac{S^2B_5+SB_6+\alpha^2}{S^2B_2+SB_3+B_4}\left[\frac{1}{S}\left(a_0+\frac{sin\phi}{F}+\frac{a_1 S}{s^2+\omega^2}\right)\right]\frac{J_1(r_n)}{r_n} \tag{34}$$

$$\therefore \overline{u_H}(r_n,s) = \left[\frac{B_9}{S-B_7}+\frac{B_{10}}{S-B_8}\right]\left[\frac{1}{S}\left(a_0+\frac{sin\phi}{F}+\frac{a_1 S}{s^2+\omega^2}\right)\right]\frac{J_1(r_n)}{r_n} \tag{35}$$

$$\therefore \overline{u_H}(r_n,s) = \left(a_0+\frac{sin\phi}{F}\right)\left[\frac{S^{-1}}{S-B_7}B_9 + \frac{S^{-1}}{S-B_8}B_{10}\right]\frac{J_1(r_n)}{r_n} + \frac{a_1 S}{s^2+\omega^2}\left[\frac{1}{S-B_7}B_9 + \frac{1}{S-B_8}B_{10}\right]\frac{J_1(r_n)}{r_n} \tag{36}$$

Where, $\overline{u_H}(r_n,s) = \int_0^1 r.\bar{u}(r,s)J_0(r_n,r)\,dr$ represents the finite Hankel transformation of the velocity and temperature function

$$\bar{u}(r,s) = LT[\bar{u}(r,t)]\,,\bar{\theta}(r,s) = LT[\bar{\theta}(r,t)] \quad and\ \bar{C}(r,s) = LT[\bar{C}(r,t)] \tag{37}$$

And $r_n, n = 1,2,3,\ldots..$ are the positive roots of an equation $J_0(x) = 0$.

The I.L.T of the image function can be written as,

$$LT^{-1}\left[\frac{1}{S^{\omega}+y}\right] = F_{\omega}(-y,t) = \sum_{n=0}^{\infty}\frac{(-y)^n t^{(n+1)w-1}}{\Gamma((n+1)w)};\ \omega > 0 \tag{38}$$

$$LT^{-1}\left[\frac{S^z}{S^w+y}\right] = R_{w,z}(-y,t) = \sum_{n=0}^{\infty}\frac{(-y)^n t^{(n+1)w-1-z}}{\Gamma((n+1)w-z)};\quad Re(w-z) > 0 \tag{39}$$

The ILT (Inverse Laplace transform) is applied in (16), (28) and (36) are

$$\therefore \overline{\theta_H}(r_n,t) = \frac{J_1(r_n)}{r_n}\left[B_{13}e^{-B_{15}t} + \frac{B_{14}}{B_{15}}(1-e^{-B_{15}t})\right] \tag{40}$$

$$\therefore \overline{C_H}(r_n,t) = \frac{J_1(r_n)}{r_n}[B_{29} + B_{30}e^{-B_{27}t} + B_{31}e^{-B_{31}t}] \tag{41}$$

$$\therefore \overline{u_H}(r_n,t) = \frac{J_1(r_n)}{r_n}\left[(e^{B_7 t}-1)\left(\frac{A_0}{B_7}B_9 + \frac{B_9 sin\phi}{B_7 F}\right) + (e^{B_8 t}-1)\left(\frac{a_0}{B_8}B_{10} + \frac{B_{10}sin\phi}{B_8 F}\right) + a_1 B_9 e^{B_7 t} * \cos(\omega t) + a_1 B_{10} e^{B_8 t} * \cos(\omega t)\right] \tag{42}$$

The exact expression of blood velocity, Temperature and Concentration profiles are obtained by taking the Inverse Hankel transformation of equations (40) - (42), we get

$$\theta(r,t) = 2\sum_{n=1}^{\infty}\frac{J_0\left(\frac{r}{r_z}r_n\right)}{r_n J_1^2(r_n)} \times \theta_H(r_n,t) \tag{43}$$

$$\theta(r,t) = 2\sum_{n=1}^{\infty}\frac{J_0\left(\frac{r}{r_z}r_n\right)}{r_n J_1^2(r_n)} \times \left[B_{13}e^{-B_{15}t} + \frac{B_{14}}{B_{15}}(1-e^{-B_{15}t})\right] \tag{44}$$

$$C(r,t) = 2\sum_{n=1}^{\infty}\frac{J_0\left(\frac{r}{r_z}r_n\right)}{r_n J_1^2(r_n)} \times C_H(r_n,t) \tag{45}$$

$$C(r,t) = 2\sum_{n=1}^{\infty}\frac{J_0\left(\frac{r}{r_z}r_n\right)}{r_n J_1^2(r_n)} \times [B_{29} + B_{30}e^{-B_{27}t} + B_{31}e^{-B_{31}t}] \tag{46}$$

$$u(r,t) = 2\sum_{n=1}^{\infty}\frac{J_0\left(\frac{r}{r_z}r_n\right)}{r_n J_1^2(r_n)} \times u_H(r_n,t) \tag{47}$$

$$u(r,t) = 2\sum_{n=1}^{\infty}\frac{J_0\left(\frac{r}{r_z}r_n\right)}{r_n J_1^2(r_n)}\left[(e^{B_7 t}-1)\left(\frac{a_0}{B_7}B_9 + \frac{B_9 sin\phi}{B_7 F}\right) + (e^{B_8 t}-1)\left(\frac{a_0}{B_8}B_{10} + \frac{B_{10}sin\phi}{B_8 F}\right) + a_1 B_9 e^{B_7 t} * \cos(\omega t) + a_1 B_{10} e^{B_8 t} * \cos(\omega t)\right] \tag{48}$$

From equation (31), we write

$$v(r,t) = B_{33}(1-B_{32})[u(r,t) * e^{B_{12}t}],\ 0 < \alpha < 1 \tag{49}$$

RESULTS AND DISCUSSION

The effects of different physical parameter on velocity, temperature and concentration profiles were studied via graphs which is represented in Fig. 2 to 14. In every case, the fractional parameter that corresponds to 1 is used for comparison, and there are very few cases in which the fractional parameter is strictly less than 1. For the numerical calculations, the following parameters are fixed. $a_0 = 0.5$, $a_1 = 0.1$, $\omega = \pi/4$, $P_e = 0.5$, G = 0.5, $H_a = 1$ and $R_e = 1$.

Figure 2-5 shows the effects of systolic and diastolic pressure gradient on both velocity profiles. From the figures, it is concluded that the blood velocity improved with both parameter values increases. Figure 6-7 shows the effects of Casson fluid parameter effects on blood as well as magnetic particle velocity. The Casson parameter is related to the non-Newtonian nature of the blood. Higher Casson parameter is attributed to the Newtonian nature. With an increase

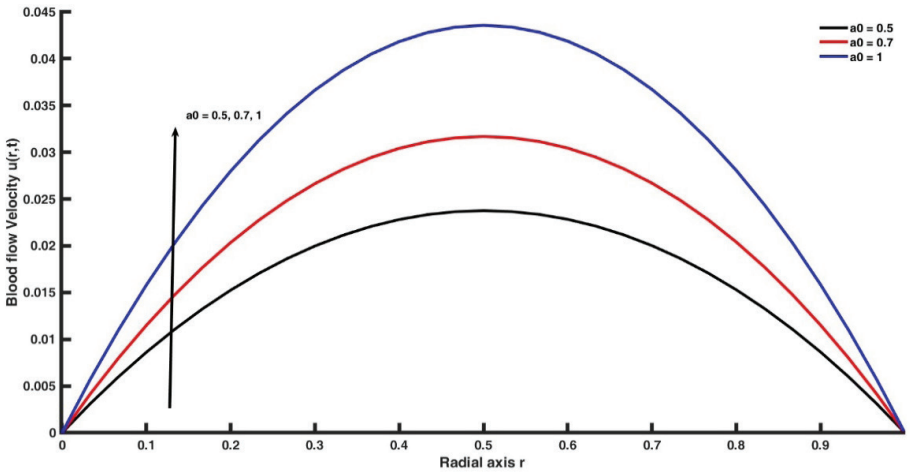

Figure 2. $u(r, t)$ for a_0.

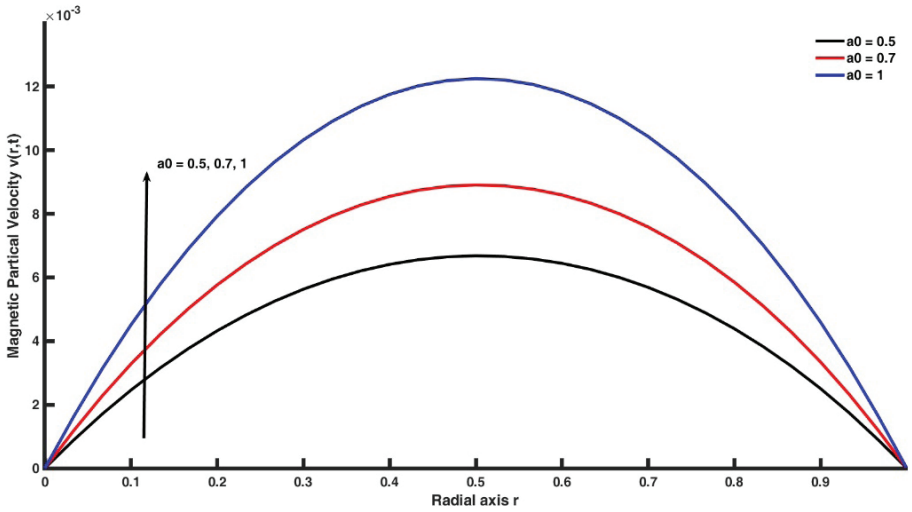

Figure 3. $v(r, t)$ for a_0.

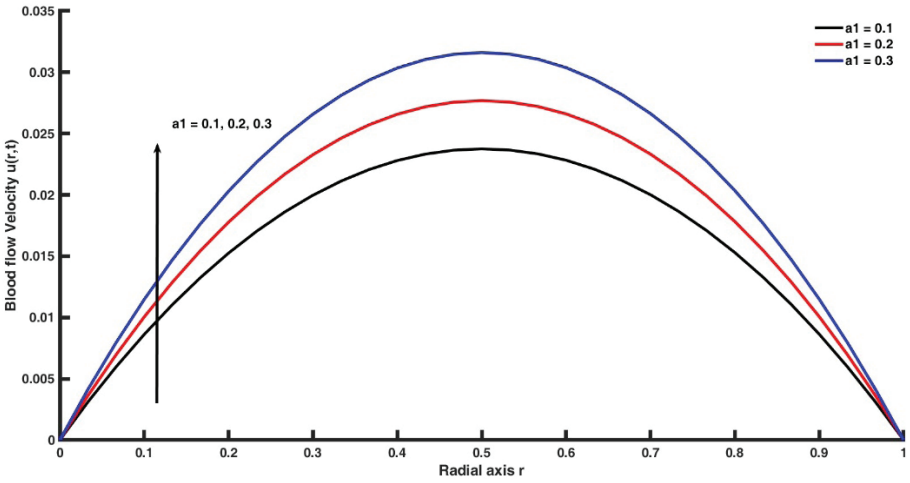

Figure 4. $u(r, t)$ for a_1.

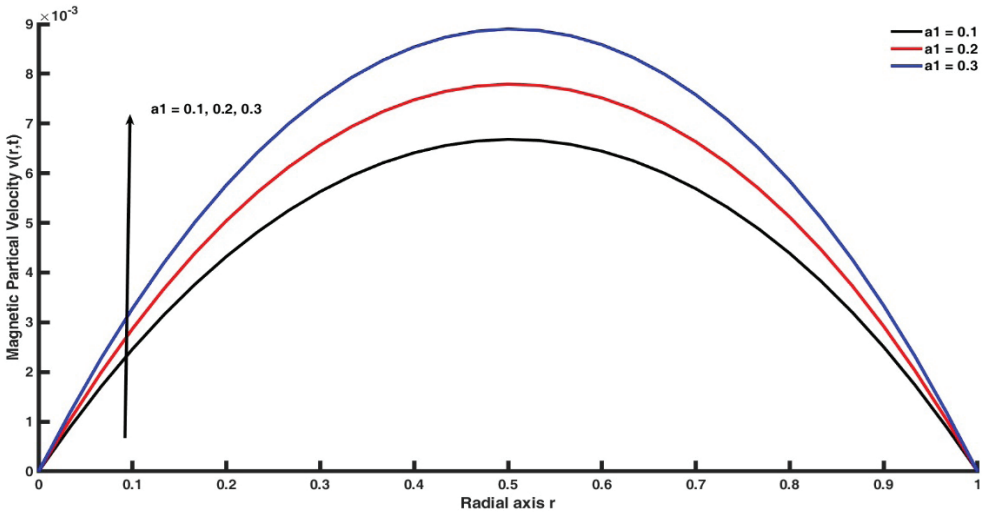

Figure 5. $v(r, t)$ for a_1.

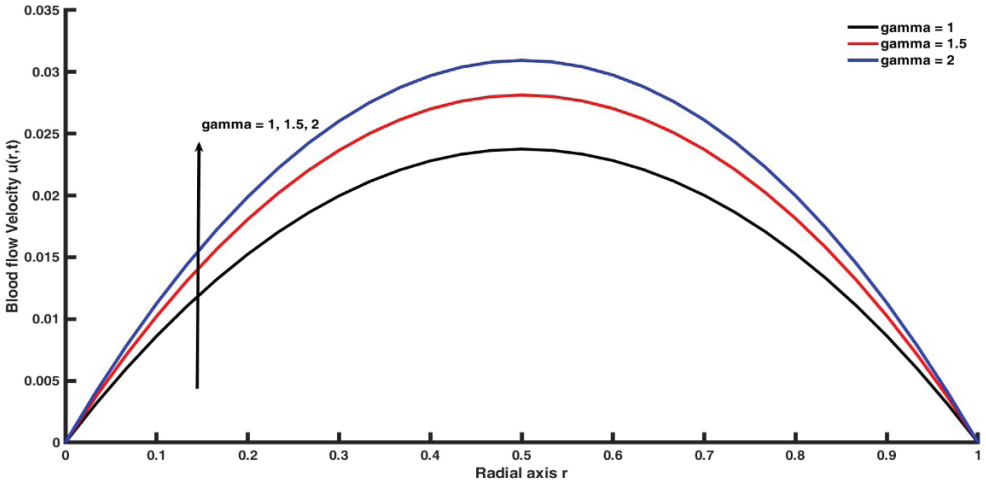

Figure 6. $u(r, t)$ for γ.

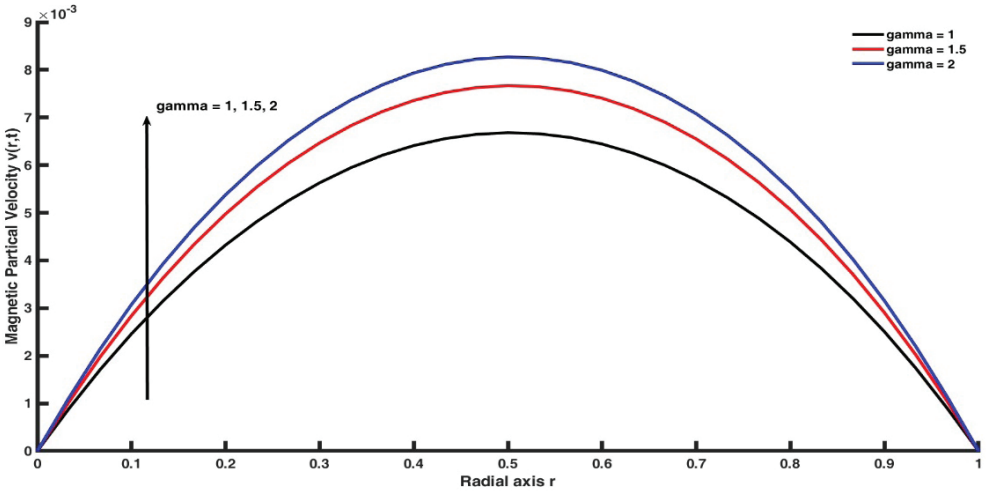

Figure 7. $v(r, t)$ for γ.

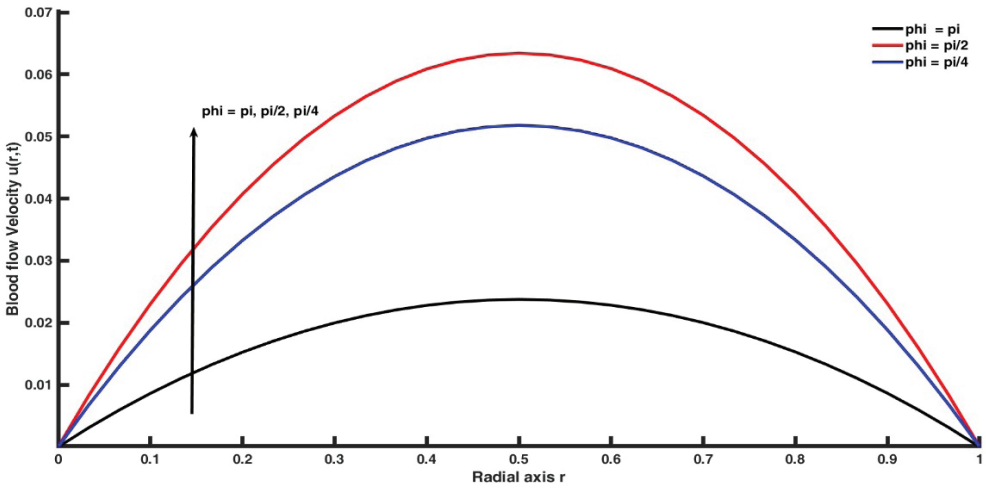

Figure 8. $u(r, t)$ for $\emptyset$.

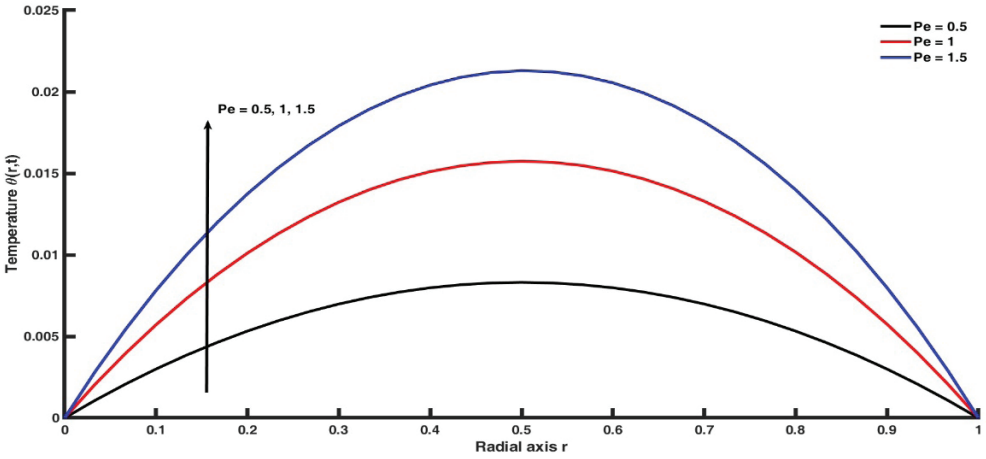

Figure 9. $\theta(r, t)$ for P_e.

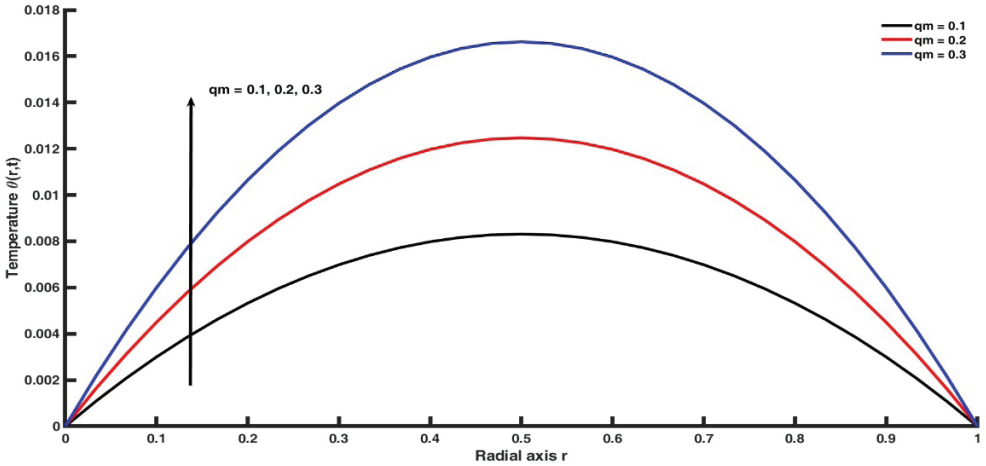

Figure 10. $\theta(r, t)$ for Q_m.

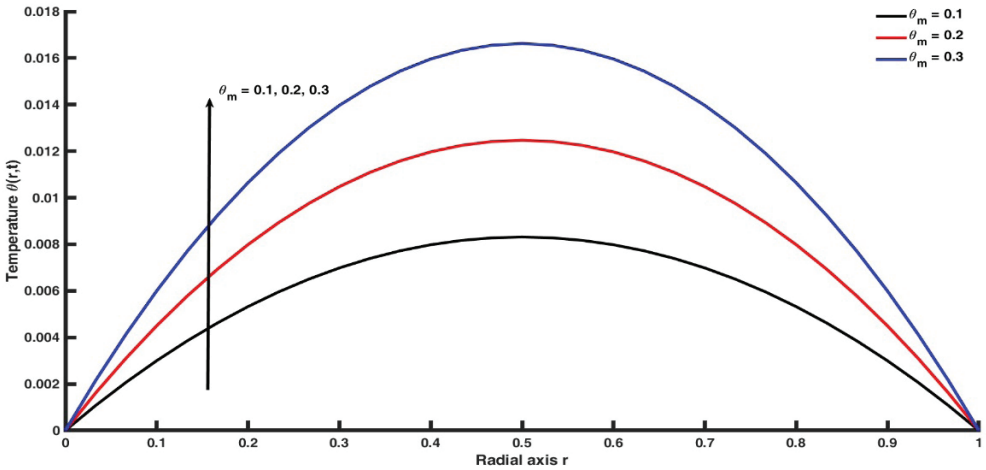

Figure 11. $\theta(r, t)$ for Q_m.

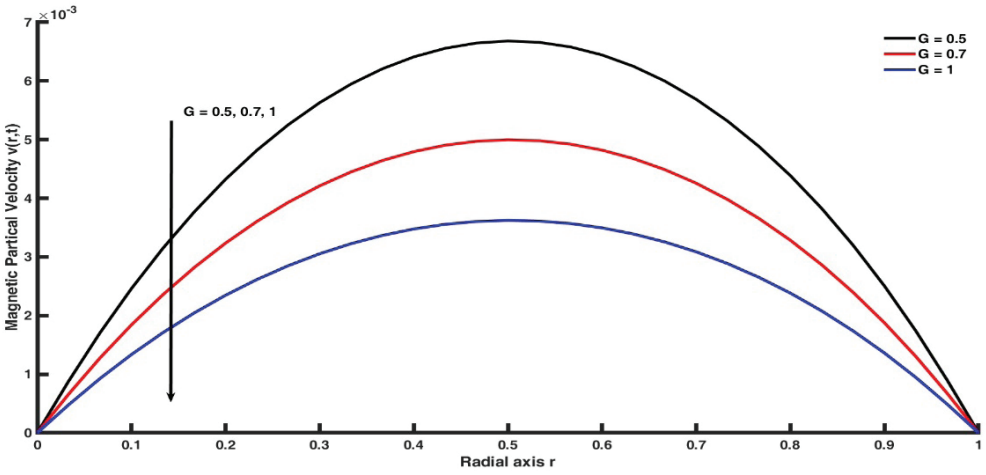

Figure 12. $v(r, t)$ for G.

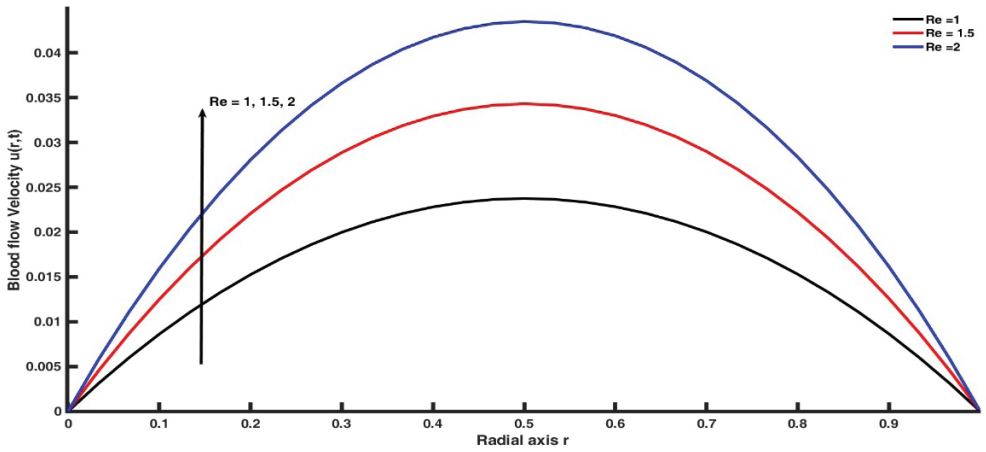

Figure 13. $u(r, t)$ for R_e.

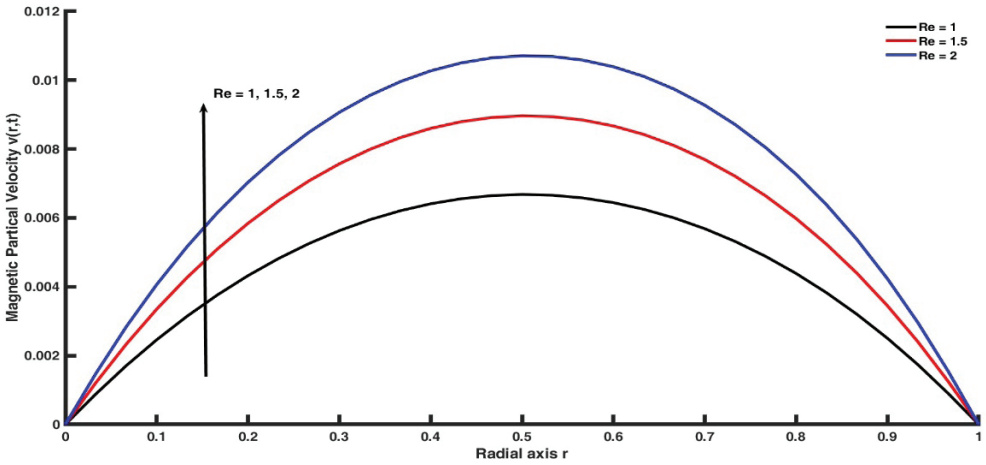

Figure 14. $v(r, t)$ for R_e.

in the Casson fluid parameter, the fluid velocity increases. Casson nature is more significant for small arteries where red blood cells (RBCs) can accumulate due to rotation near the axis of the artery, creating a region depicted in the cells. This statement is in perfect agreement with Jamil et al., [34] for a horizontal cylinder. It is hypothesized that the yield stress declines as γ increases and the thickness of the boundary layer decreases. The magnetic field is used for regulating the blood flow within the human circulatory system. Due to increasing the values of Casson fluid parameter values, blood become thin, so the motion of flow is improved. The blood velocity at different inclination angles ∅ are plotted in Figure 8. From the figure, inclination angles tend to improve the velocity profiles. Figure 9 show the temperature profiles increase with increasing the values Peclet number.

Figure 10-11 show the effects of metabolic heat source and heat absorption parameter on temperature profiles. From both figures, it is illustrated that the heat transfer process improves with both parameters. Physically when we increase the heat source parameter, fluid become thinner, due to this effects heat transfer process become faster. The particle mass parameter G is defined as the size of the particles. Figure 12 shows the effects of mass parameter on magnetic particle velocity. From the figure, it is seen that the magnetic particle velocity reduces with increasing the values of said parameter. Figure 13-14 displayed the Reynolds numbers effects on both velocity profiles. Physically, lower viscosity (increased velocity) will increase. So, from the both figures, it is concluded that the blood as well as magnetic fields velocity improved with increasing the values of Reynolds number.

CONCLUSION

The following are the most significant findings:

- The blood flow and magnetic particles distributions are highly influenced by the fractional order parameter. It should be noted that the particle has the same tendency as the blood; however, it moves slower.
- The magnetic particle velocity is slow compared to the blood velocity. These findings will be beneficial for atherosclerosis therapy.
- The blood as well as magnetic particle velocity improved with Reynold number and Casson fluid parameter.
- The numerical findings reveal that the inclination angle has a considerable influence on blood and magnetic particle velocities. The development might help in identifying and treatment for specific illnesses.
- The systolic and diastolic pressure gradients tend to raise blood flow and magnetic particle velocity. Because of these consequences, blood flow in the stenosis artery may be normal.
- The Peclet number tends to improve heat transfer process.

ACKNOWLEDGEMENT

Authors are thankful to Ganpat University- Centre for Advanced Research Studies (CARS) (F. No. 273/GUNI/CARS/1309/2022, Date: 21/10/2022) for providing financial support to carry out research work.

AUTHORSHIP CONTRIBUTIONS

Authors equally contributed to this work.

DATA AVAILABILITY STATEMENT

The authors confirm that the data that supports the findings of this study are available within the article. Raw data that support the finding of this study are available from the corresponding author, upon reasonable request.

CONFLICT OF INTEREST

The author declared no potential conflicts of interest with respect to the research, authorship, and/or publication of this article.

ETHICS

There are no ethical issues with the publication of this manuscript.

STATEMENT ON THE USE OF ARTIFICIAL INTELLIGENCE

Artificial intelligence was not used in the preparation of the article.

NOMENCLATURE

B_0	Magnetic field parameter
γ	Casson parameter
ω	"Pulsatile frequency"
R	Particle concentration parameter"
H_a	Magnetic field parameter
$\emptyset$	Phase angle
F	Inclination angle
P	Oscillating pressure gradient
R_e	Reynolds number
P_e	Peclet Number
Q_m	Heat Source
θ_m	Heat absorption
G	Particle mass parameter
ρ	Fluid density
r	Radial coordinator
α	Fractional parameter
σ	Electrical conductivity
$u(r, t)$	velocity of the Fluid
$v(r, t)$	velocity of the Particle
θ	Dimensionless Temperature
N	Magnetic particles number
K	Stokes constant
υ	Kinematic viscosity
S_c	Schmidt number
S_r	Soret parameter

REFERENCES

[1] Casson N. Flow equation for pigment-oil suspensions of the printing ink-type. Rheol Disperse Syst 1959:84–104.

[2] Young DF, Tsai FY. Flow characteristics in models of arterial stenoses—I. Steady flow. J Biomech 1973;6:395–410. [CrossRef]

[3] Young DF, Tsai FY. Flow characteristics in models of arterial stenoses—II. Unsteady flow. J Biomech 1973;6:547–559. [CrossRef]

[4] Misra JC, Patra MK, Misra SC. A non-Newtonian fluid model for blood flow through arteries under stenotic conditions. J Biomech 1993;26:1129–1141. [CrossRef]

[5] Massoudi M, Phuoc TX. Pulsatile flow of blood using a modified second-grade fluid model. Comput Math Appl 2008;56:199–211. [CrossRef]

[6] Chaturani P, Ponnalagar Samy R. A study of non-Newtonian aspects of blood flow through stenosed arteries and its applications in arterial diseases. Biorheology 1985;22:521–531. [CrossRef]

[7] Alfvén H, Arrhenius G. Structure and evolutionary history of the solar system, I. Astrophys Space Sci 1970;8:338–421. [CrossRef]

[8] Rashidi S, Esfahani JA, Maskaniyan M. Applications of magnetohydrodynamics in biological systems-a review on the numerical studies. J Magn Magn Mater 2017;439:358–372. [CrossRef]

[9] Liu J, Flores GA, Sheng R. In-vitro investigation of blood embolization in cancer treatment using magnetorheological fluids. J Magn Magn Mater 2001;225:209–217. [CrossRef]

[10] Prasad NK, Rathinasamy K, Panda D, Bahadur D. Mechanism of cell death induced by magnetic hyperthermia with nanoparticles of γ-MnxFe2−xO3 synthesized by a single step process. J Mater Chem 2007;17:5042–5051. [CrossRef]

[11] Shih TC, Kou HS, Lin WL. Effect of effective tissue conductivity on thermal dose distributions of living tissue with directional blood flow during thermal therapy. Int Commun Heat Mass Transf 2002;29:115–126. [CrossRef]

[12] Mekheiner KS, El Kot MA. Suspension model for blood flow through catheterized curved artery with time-variant overlapping stenosis. Eng Sci Technol Int J 2015;18:452–462. [CrossRef]

[13] Majee S, Shit GC. Numerical investigation of MHD flow of blood and heat transfer in a stenosed arterial segment. J Magn Magn Mater 2017;424:137–147. [CrossRef]

[14] Rao PS, Rao JA. Numerical solution of non-steady magnetohydrodynamic flow of blood through a porous channel. J Biomed Eng 1988;10:293–295. [CrossRef]

[15] Shah NA, Vieru D, Fetecau C. Effects of the fractional order and magnetic field on the blood flow in cylindrical domains. J Magn Magn Mater 2016;409:10–19. [CrossRef]

[16] Baleanu D, Agrawal OP. Fractional Hamilton formalism within Caputo's derivative. Czech J Phys 2006;56:1087–1092. [CrossRef]

[17] Odibat Z. Approximations of fractional integrals and Caputo fractional derivatives. Appl Math Comput 2006;178:527. [CrossRef]

[18] Mekheimer KS. Peristaltic flow of blood under effect of a magnetic field in a non-uniform channel. Appl Math Comput 2004;153:763–777. [CrossRef]

[19] Akbar NS. Blood flow analysis of Prandtl fluid model in tapered stenosed arteries. Ain Shams Eng J 2014;5:1267–1275. [CrossRef]
[20] Sreenadh S, Komala K, Srinivas ANS. Peristaltic pumping of a power–Law fluid in contact with a Jeffrey fluid in an inclined channel with permeable walls. Ain Shams Eng J 2017;8:605–611. [CrossRef]
[21] Ramesh K, Devakar M. Some analytical solutions for flows of Casson fluid with slip boundary conditions. Ain Shams Eng J 2015;6:967–975. [CrossRef]
[22] Mahboobtosi M, Hosseinzadeh K, Ganji DD. Entropy generation analysis and hydrothermal optimization of ternary hybrid nanofluid flow suspended in polymer over curved stretching surface. Int J Thermofluids 2023;20:100507. [CrossRef]
[23] Moghimi SM, Hosseinzadeh K, Hasibi A. Investigation of nanofluid flow in the channel under effect of magnetic field and joule heating. Case Stud Therm Eng 2024;55:104152. [CrossRef]
[24] Akbari S, Farahani MF, Hosseinzadeh K. Theoretical analysis of transient counter-flow combustion system fueled by porous biomass particles in a non-premixed configuration under non-adiabatic conditions. Int J Thermofluids 2024;22:100653. [CrossRef]
[25] Alipour N, Jafari B, Hosseinzadeh K. Optimization of wavy trapezoidal porous cavity containing mixture hybrid nanofluid (water/ethylene glycol Go–Al2O3) by response surface method. Sci Rep 2023;13:1635. [CrossRef]
[26] Zangooee MR, Hosseinzadeh K, Ganji DD. Hydrothermal analysis of Ag and CuO hybrid NPs suspended in mixture of water 20%+ EG 80% between two concentric cylinders. Case Stud Therm Eng 2023;50:103398. [CrossRef]
[27] Hosseinzadeh S, Hosseinzadeh K, Hasibi A, Ganji DD. Thermal analysis of moving porous fin wetted by hybrid nanofluid with trapezoidal, concave parabolic and convex cross sections. Case Stud Therm Eng 2022;30:101757. [CrossRef]
[28] Hosseinzadeh K, Afsharpanah F, Zamani S, Gholinia M, Ganji DD. A numerical investigation on ethylene glycol-titanium dioxide nanofluid convective flow over a stretching sheet in presence of heat generation/absorption. Case Stud Therm Eng 2018;12:228–236. [CrossRef]
[29] Gulzar MM, Aslam A, Waqas M, Javed MA, Hosseinzadeh K. A nonlinear mathematical analysis for magneto-hyperbolic-tangent liquid featuring simultaneous aspects of magnetic field, heat source and thermal stratification. Appl Nanosci 2020;10:4513–4518. [CrossRef]
[30] Faghiri S, Akbari S, Shafii MB, Hosseinzadeh K. Hydrothermal analysis of non-Newtonian fluid flow (blood) through the circular tube under prescribed non-uniform wall heat flux. Theor Appl Mech Lett 2022;12:100360. [CrossRef]
[31] Tashtoush B, Magableh A. Magnetic field effect on heat transfer and fluid flow characteristics of blood flow in multi-stenosis arteries. Heat Mass Transf 2008;44:297–304. [CrossRef]
[32] Dzuliana FJ, Salah U, Rozaini R. The effects of magnetic Casson blood flow in an inclined multi-stenosed artery by using Caputo-Fabrizio fractional derivatives. J Adv Res Mater Sci 2020;72:15–30. [CrossRef]
[33] Ali F, Sheikh NA, Khan I, Saqib M. Magnetic field effect on blood flow of Casson fluid in axisymmetric cylindrical tube: A fractional model. J Magn Magn Mater 2017;423:327–336. [CrossRef]
[34] Dzuliana FJ, Salah U, Muhamad GK, Rozaini R. The effects of magnetic Casson blood flow in an inclined multi-stenosed artery by using Caputo-Fabrizio fractional derivatives. J Adv Res Fluid Mech Therm Sci 2021;82:28–38. [CrossRef]

APPENDIX

$B_1 = R + Ha^2 + \gamma {r_n}^2$

$B_2 = 1 + G - \alpha - R - R\alpha^2 + 2R\alpha + B_1 + B_1\alpha^2 - 2\alpha B_1 + GB_1 - G\alpha B_1$

$B_3 = \alpha + 2R\alpha^2 - 2R\alpha - 2B_1\alpha^2 + 2\alpha B_1 + G\alpha B_1$

$B_4 = B_1\alpha^2 - R\alpha^2, B_5 = 1 + \alpha^2 - 2\alpha + G + G\alpha\,, B_6 = -2\alpha^2 + 2\alpha + G\alpha$

$B_7 = \frac{-B_3 \pm \sqrt{{B_3}^2 - 4B_2B_4}}{2B_2}, B_8 = \frac{-B_3 \pm \sqrt{{B_3}^2 - 4B_2B_4}}{2B_2}, B_9 = \frac{{B_7}^2B_5 + B_7B_6 + \alpha^2}{B_7 - B_8},$

$B_{10} = \frac{{B_8}^2B_5 + B_8B_6 + \alpha^2}{B_8 - B_7}, B_{11} = (r_n)(1-\alpha) + P_e, B_{12} = (r_n).\alpha$

$B_{13} = P_e\frac{(Q_m + \theta_m)(1-\alpha)}{B_{11}}, B_{14} = P_e\frac{(Q_m + \theta_m).\alpha}{B_{11}}, B_{15} = \frac{B_{12}}{B_{11}},$

$B_{16} = -S_r\,S_c\,r_nP_e\,(Q_m + \theta_m), B_{17} = r_n, B_{18} = r_n$

$B_{19} = R_eS_c\,, B_{20} = B_{17} - B_{17}\alpha + P_e, B_{21} = B_{19} + B_{18} - B_{18}\alpha, B_{22} = B_{17}\alpha$

$B_{23} = B_{18}\alpha, B_{24} = \frac{B_{16}}{B_{20}.B_{21}}, B_{25} = 2\alpha(1-\alpha), B_{26} = (1-\alpha)^2, B_{27} = \frac{B_{22}}{B_{20}}$

$B_{28} = \frac{B_{23}}{B_{21}}, B_{29} = \frac{B_{24}(\alpha^2)}{B_{27}B_{28}}, B_{30} = \frac{B_{24}\left(\alpha^2 + B_{25}(-B_{27}) + B_{26}(B_{27})^2\right)}{(-B_{27})(B_{28} - B_{27})},$

$B_{31} = \frac{B_{24}\left(\alpha^2 + B_{25}(-B_{28}) + B_{26}(B_{28})^2\right)}{(-B_{28})(B_{27} - B_{28})}\,, B_{32} = \frac{1-\alpha}{G-\alpha+1}\,, \quad B_{33} = \frac{\alpha}{G-\alpha+1}$

$f * g -$ convolution of f & g , $f * g = \int_0^t f(z)g(t-z)dz$